Supplemental material for "Rotating atomic quantum gases with light-induced azimuthal gauge potentials and the observation of Hess-Fairbank effect"

P. -K. Chen,[1] L. -R. Liu,[1] M. -J. Tsai,[1] N. -C. Chiu,[1] Y. Kawaguchi,[2] S. -K. Yip,[1,3,4] M. -S. Chang,[1] and Y. -J. Lin[1,*]

[1] *Institute of Atomic and Molecular Sciences, Academia Sinica, Taipei, Taiwan 10617*
[2] *Department of Applied Physics, Nagoya University, Nagoya, 464-8603, Japan*
[3] *Institute of Physics,Academia Sinica, Taipei, Taiwan 11529*
[4] *National Center for Theoretical Sciences, Hsinchu, Taiwan 300*

(Dated: October 25, 2018)

TDGPE SIMULATIONS

We numerically simulate the dynamics by solving the three-component 3D time-dependent-Gross-Pitaevskii equation (TDGPE). This includes the kinetic energies, quadratic Zeeman energy, mean field interaction parameters $c_0 = 4\pi\hbar^2(a_0 + 2a_2)/3m$ and $c_2 = 4\pi\hbar^2(a_2 - a_0)/3m < 0$, where a_f is the s-wave scattering length in the total spin f channel [**?**].

We use the Crank-Nicolson method and calculate in the system size of $(256)^3$ grid points with grid size 0.16 μm. During TOF, we solve the full 3D TDGPE for up to ≤ 4 ms at which the interatomic interaction energy becomes less than 3 percent of the total energy. The further evolution is calculated by neglecting the interaction term. The results for the lowest energy dressed state with a short hold time $t_h = 1$ ms are shown in Fig. S1; our corresponding data is in Fig. 2. Using the loaded atomic state from TDGPE at $\delta = 0$, the probability of projection to the local dressed state $|\xi_{-1}\rangle$ is ≥ 0.99 at $r \geq r_c = 1.8$ μm.

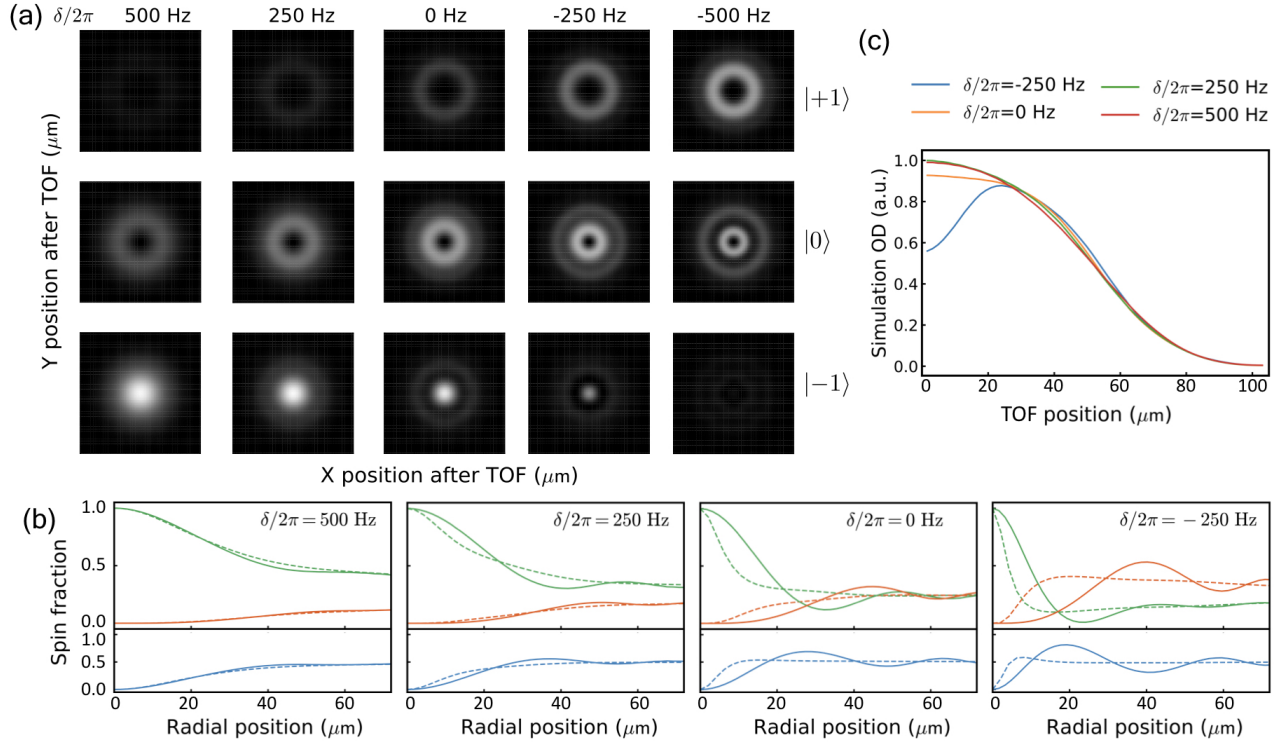

FIG. 1: 3D TDGPE simulation results for the BEC loaded into the $\ell = \hbar$ lowest energy dressed state at various detuning δ with a hold time $t_h = 1$ ms. (a) Absorption images D_{m_F} after a 24 ms TOF. The image field of view is 200×200 μm. (b) Spin texture $D_{m_F}/(D_1 + D_0 + D_{-1})$ vs. radial position. Dashed curves denote the in-situ profile after a $r \to r/13.0$ magnification; solid curves denote those after a 24 ms TOF. Green, orange and blue curves denote $|-1\rangle, |1\rangle, |0\rangle$, respectively. (c) total optical density $(D_1 + D_0 + D_{-1})$ for simulated TOF profiles.

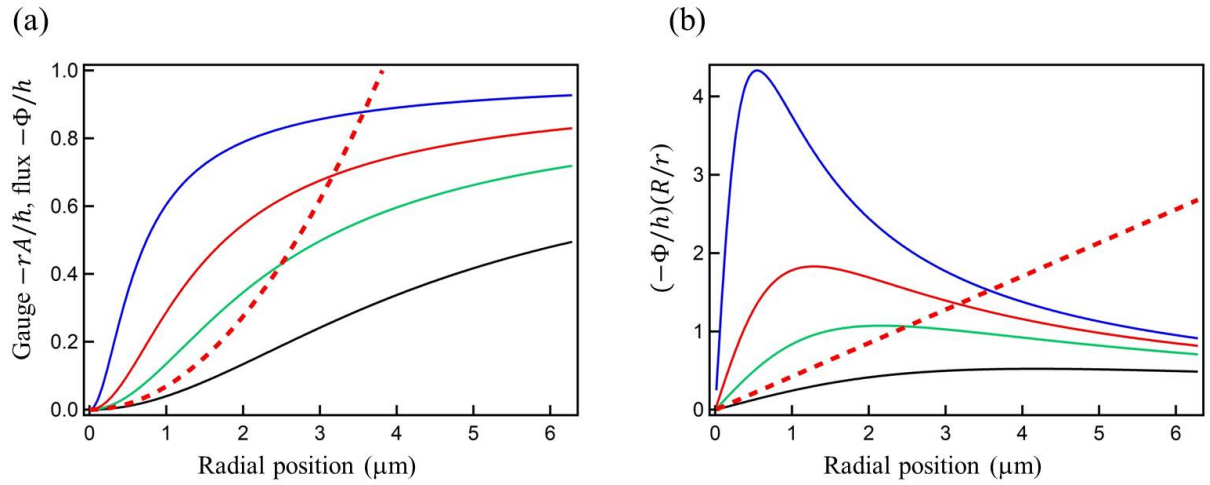

FIG. 2: (a) Gauge potential $-rA^+_{-1}/\hbar$, which is equal to the flux $-\Phi/h$, versus radial position r. Black, green, red and blue solid curves denote the lowest energy dressed state with $\delta/2\pi = 1000, 500, 295, 125$ Hz, respectively. $\delta_c/2\pi = 295$ Hz is the critical detuning. Red dashed curve represents the mechanically rotating BEC with the critical frequency ω_c. (b) $-(\Phi/h)(R/r)$ versus r. Symbols represent the same as those in (a).

SYNTHETIC MAGNETIC FLUX OF DRESSED ATOMS

We compare the thermodynamic ground state of the dressed atoms in $|\xi_{-1}\rangle$ under synthetic magnetic fields to that of mechanically rotating BECs. Taking $\delta > 0$ where $\vec{B}^* \cdot \mathbf{e}_z < 0$ as the example, we consider the azimuthal kinetic energy in Eq. (1), which is gauge invariant and can be written as $(\ell^+ - rA^+_{-1})^2/2mr^2$ in the gauge of Eq. (4). Here we simplify the calculation by assuming a disk BEC geometry, although our BEC is 3D and has a Thomas-Fermi (TF) profile. Similar calculations for 3D TF BECs are shown in Ref. [**?**]. The contribution to the kinetic energy per atom is

$$\begin{aligned}&\frac{1}{\pi R^2}\int_0^R dr2\pi r\frac{(\ell^+ - rA^+_{-1})^2}{2mr^2}\\&= \frac{1}{\pi R^2}\left[\int dr2\pi r\frac{(\ell^+)^2}{2mr^2} - \int dr2\pi r\frac{\ell^+\hbar}{mr^2}(\cos\beta - 1) + \int dr2\pi r\frac{\left(rA^+_{-1}\right)^2}{2mr^2}\right].\end{aligned} \tag{1}$$

With $\delta > 0$, $\cos\beta - 1$ is negative. We thus compare the energy with $\ell^+ = 0$ and with $\ell^+ = -\hbar$, where the lower one is the ground state. The energy for $\ell^+ = -\hbar$ relative to $\ell^+ = 0$ is

$$E_{B^*} = \frac{1}{\pi R^2}\int_{r_v}^R dr2\pi r\frac{\hbar^2}{2mr^2} + \frac{1}{\pi R^2}\int_0^R dr2\pi r\frac{\hbar^2}{mr^2}(\cos\beta - 1), \tag{2}$$

where the first term is the vortex kinetic energy E_v and r_v is the vortex core size. At large δ, $\cos\beta - 1 \approx 0$ and $E_{B^*} \approx E_v$, leading to the $\ell^+ = 0$ ground state. As δ decreases, $|\cos\beta - 1|$ increases, and the ground state makes a transition to $\ell^+ = -\hbar$ when the absolute value of the second therm in Eq. S(2) equals E_v.

Then we analogously consider a mechanically rotating BEC with angular frequency $-\omega$, where $\omega > 0$. The kinetic energy for $\ell = -\hbar$ relative to $\ell = 0$ is

$$\begin{aligned}E_{\rm mech} &= \frac{1}{\pi R^2}\int_{r_v}^R dr2\pi r\frac{\hbar^2}{2mr^2} - \frac{1}{\pi R^2}\int_0^R dr2\pi r\frac{\hbar^2}{mr^2}\frac{m\omega r^2}{\hbar}\\&= E_v - \frac{1}{\pi R^2}\int_0^R dr2\pi r\hbar\omega.\end{aligned} \tag{3}$$

The critical angular frequency for the ground state changes from $\ell^+ = 0$ to $\ell^+ = -\hbar$ with increasing ω is $\omega_c = \hbar/(mR^2)\ln(R/r_v)$.

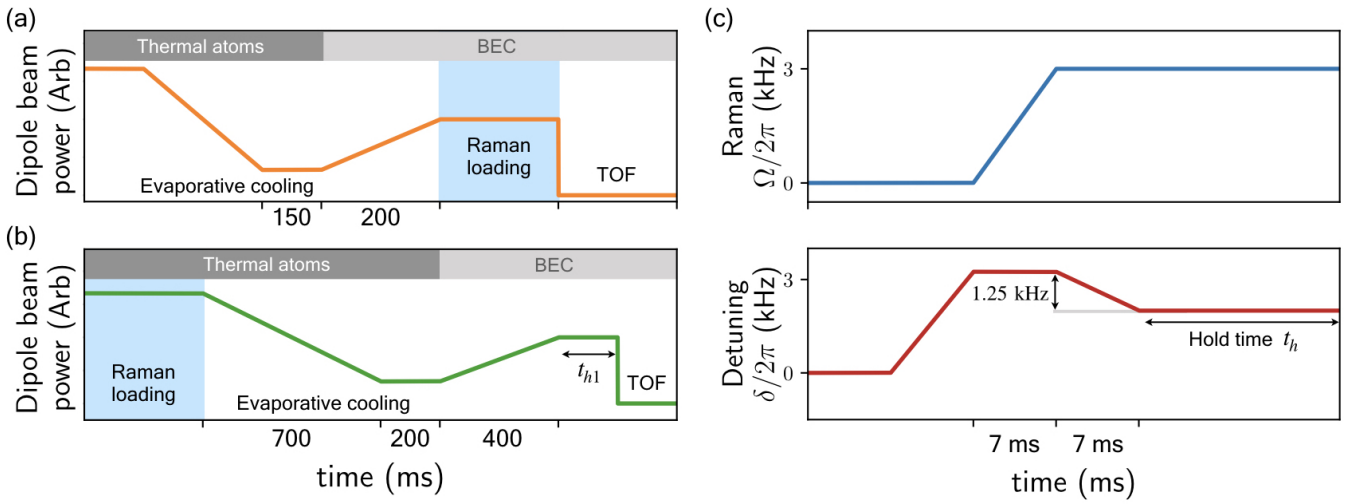

FIG. 3: Time sequences of the experiment. (a) Dipole beam power in the procedure for the coreless vortex data in Fig. 2. (b) Dipole beam power in the procedure for data in Fig. 4 showing Hess-Fairbank effect. (c) The sequences of Raman loading in (a) and (b).

To compare the dressed atoms and the mechanically rotating BEC, we consider the dimensionless gauge potential $rA/\hbar$, which is equal to the flux Φ enclosed by radius r in unit of h [see Eq. (4)], given that $\oint \vec{A}\cdot\vec{dl} = A(r)2\pi r = \Phi$; Φ represents $\Phi^{+}_{B^*}$ and $\Phi_{\rm mech}$. We then plot $rA^{+}_{-1}/\hbar = \cos\beta(r) - 1$ and $m\omega_c r^2/\hbar$ versus r in Fig. S2a, showing curves of $\cos\beta(r) - 1$ with various detuning $\delta/2\pi$ for the dressed atoms. Here we use $r_v = 0.5$ μm for both Eq. S(2) and Eq. S(3), and thus $\omega_c/2\pi = 8.0$ Hz for the TF radius $R \approx 6$ μm. We derive r_v for dressed atoms from the projection probability of the spinor wave function of the absolute ground state with $\ell^{+} = -\hbar$ (i.e., $\ell = 0$) onto $|\xi_{-1}\rangle$, where Eq. S(1) applies. This probability is zero at $r = 0$ and increases with increasing r, and we take r_v as the radial position with the probability of 0.65. We find $r_v \sim 0.5$ μm is approximately independent of δ for 125 Hz$< \delta/2\pi <$ 300 Hz.

From Fig. S2a, we observe the flux enclosed by $r = R$ is $|\Phi_{\rm mech}|/h \approx 2.6 > 1$ while $|\Phi^{+}_{B^*}|/h < 1$ is limited by our $\Delta\ell = \hbar$. Since E_v is the same in Eq. S(2) and Eq. S(3), we then compare the integrand of the second term in Eq. S(2) and Eq. S(3), respectively, versus r in Fig. S2b, which are contributed from the gauge potential rA^{+}_{-1} and $m\omega_c r^2$. The integrand is scaled as $(\Phi/h)(R/r)$. At the critical detuning δ_c for the dressed atoms, the quasi-angular momentum $\ell^{+} = \ell - \hbar$ of the ground state changes from 0 to $-\hbar$. We determine δ_c from Fig. S2b, where the enclosed area by the red curve denoting δ_c equals to that of the red-dashed curve representing the mechanically rotating BEC with the critical frequency ω_c. We find this condition is fulfilled at $\delta_c/2\pi \approx 295$ Hz. Fig. S2a shows that at small r the gauge potential $|rA_{-1}|$ of dressed atoms with $\delta/2\pi \leq 500$ Hz is larger than the $m\omega_c r^2$ for the mechanical rotation; the contribution at small r is further enhanced by the $2\pi\hbar^2/(mr)$ factor in the integrand (see Fig. S2b). Therefore, the critical flux for the symmetric gauge is $|\Phi_{\rm mech}|/h > 1$ while $|\Phi^{+}_{B^*}|/h \approx 0.8 < 1$ for our dressed atoms.

EXPERIMENTAL SETUP AND PROCEDURES

For the coreless vortex data in Fig. 2, we first produce a ^{87}Rb BEC and then load it into the Raman-dressed state $|\xi_{-1}\rangle$. We achieve a BEC of $N \approx 1.2\times10^5$ atoms in a crossed dipole trap in $|F, m_F\rangle = |1,-1\rangle$ [**?**]. The dipole trap contains two 1064 nm laser beams propagating along $\mathbf{e}_{x'}, \mathbf{e}_{y'} = (\mathbf{e}_x \pm \mathbf{e}_y)/\sqrt{2}$ with beam waists of ~ 30 μm. After the forced evaporation and a 1.5 s free evaporation, the dipole beam powers are ramped up in 0.2 s in order to reach the final trap frequencies of $(\omega_{x'}, \omega_{y'}, \omega_z)/2\pi$=(140,140,190) Hz. The radial trap frequency is chosen such that it is sufficient for the atoms to sustain a Thomas-Fermi profile in the presence of the anti-trapping light shift potential near Raman resonance, $-\sqrt{\Omega(r)^2 + \delta^2}$.

After the BEC preparation we wait for the external trigger from the 60 Hz line, after which we apply feed-forward current signals into bias coils to cancel the field noise from 60 Hz harmonics (see later discussions). Then we load the $|m_F = -1\rangle$ BEC into the lowest energy dressed state $|\xi_{-1}\rangle$ with the following procedures. We ramp the detuning to $\delta/2\pi = \delta_f/2\pi + 1.25$ kHz while the Raman beams are off, ramp $\Omega(r,t)$ in 7 ms to the final value of $\Omega_M/2\pi = 3.0$ kHz, and then ramp the detuning to $\delta_f/2\pi$ between 500 Hz and -500 Hz in 7 ms (see Fig. S3), subsequently holding Ω_M and δ at constant for t_h. The Raman beams are at $\lambda = 790$ nm where their scalar light shifts from the D1 and

D2 lines cancel. The Gaussian Raman beam has a waist of 200 μm, and the LG Raman beam produced by a vortex phase plate has a phase winding number $m_\ell = 1$ and radial index of 0. The Raman beams are linearly polarized along $\mathbf{e}_x$ and $\mathbf{e}_y$, respectively.

To show the Hess-Fairbank effect in Fig. 4, we start with thermal atoms right above the BEC transition temperature, load to the dressed state $|\xi_{-1}\rangle$ using the same sequence as that for data in Fig. 2. Next we force evaporatively cool the atoms to achieve BECs and hold 0.2 s for free evaporation, then increase the dipole beam powers in 0.4 s to reach the trap frequencies $(\omega_{x'}, \omega_{y'}, \omega_z)$, subsequently holding for t_{h1} before TOF. To reduce the shot-to-shot field noise when TOF starts, we wait for the 60 Hz line trigger at 20 ms before the TOF. This adds to t_{h1} by a varying time up to 16.7 ms (period of 60 Hz) as the experiment is repeated.

For projection measurements of the spinor state $|\xi_s\rangle$, we abruptly turn off the dipole trap and Raman beams, simultaneously and adiabatically rotate the magnetic bias field from along $\mathbf{e}_x$ to that along the imaging beam direction within 0.4 ms. The spinor wave function is then projected to the bare spin m_F basis. For data in Fig. 2 and Fig. 4, the atoms then expand in free space with all m_F components together for a TOF. To perform spin-selective imaging, we apply microwave spectroscopy for imaging each $|m_F\rangle$ [**?**]. Each $|m_F\rangle$ image is obtained in an individual experimental realization. After the $F = 1$ atoms are transferred to $F = 2$ by the microwave pulses, we apply a resonant absorption imaging pulse of ~ 14 μs with $\sigma+$ polarization at the $|F = 2, m_F = 2\rangle \rightarrow |F^{'} = 3, m_F = 3\rangle$ cycling transition. With our $I/I_{\rm sat}$ parameters, we use the modified Beer-Lamberet law [**?**] to derive correct optical densities. For data in Fig. 3, we apply a Stern-Gerlach field gradient to spatially separate individual $|m_F\rangle$ states during TOF, then a $F = 1 \rightarrow F^{'} = 2$ repumping pulse is applied, after which the images of all $|m_F\rangle$ states are taken in a single shot.

We characterize the ambient field noise after the external trigger from the 60 Hz line. The noise is dominated by the 60 Hz line signal with a standard deviation (σ) of $\sim h \times 300$ Hz. After we apply feed-forward signals in the bias fields to cancel the dominating field noise at 60 Hz, the $1-\sigma$ residual field noise can be reduced to $h \times 120$ Hz within 0.4 s after the 60 Hz trigger, in the best case. For longer time the 60 Hz line has a phase decoherence and the feed-forward cancelation does not work. For the data in Fig. 2 where the Raman loading takes 14 ms, we prepare the dressed state after the 60 Hz line trigger in order to reduce the shot-to-shot field variation with a fixed time after the trigger, and the measured $1-\sigma$ field noise from repeated experimental shots is $\sim h \times 70$ Hz.

DATA ANALYSIS

For data in Fig. 2, we average over 4 to 5 images for each δ taken under identical conditions. We post-select images whose vortex positions in $|m_F = \pm 1\rangle$ with respect to the BEC center are < 0.3 μm (converted from TOF position to the in-situ position). We determine $\delta/2\pi$ from the rf-spectroscopy with an uncertainty of ≈ 20 Hz. The uncertainty of the spin fraction displayed in Fig. 2b is $\sigma/\sqrt{N}$, where σ is the standard deviation of pixels along $\mathbf{e}_\phi$ at a fixed r, and $N = 4$ or 5 is the number of images.

For data in Fig. 4, the variations in the winding number of $|m_F = 0\rangle$ component within 20 identical experimental realizations are most likely due to the detuning noise. Thus, in the images at $\delta/2\pi = 50$ Hz with $\langle|\ell_g|\rangle/\hbar \sim 0$, for $|m_F = 0\rangle$ component we post-select those with no hole corresponding to $\ell_g = 0$. For $|m_F = 1\rangle$ component we select those with smaller holes corresponding to $\ell_g + \hbar = \hbar$ and excluding those with larger holes corresponding to $\ell_g + \hbar = 2\hbar$. Similarly, we post-select those with $\ell_g - \hbar = -\hbar$ in $|m_F = -1\rangle$ with $\delta/2\pi = 50$ Hz, and further select those with $\ell_g = \hbar$ for $|m_F = 0, \pm 1\rangle$ images with $\delta/2\pi = 400$ Hz based on the hole size in the images. For both $\delta/2\pi = 50, 400$ Hz, each m_F state image is a single-shot image.

In the Hess-Fairbank effect experiment, we consider the effects of the dominating detuning noise at 60 Hz with an amplitude of $\approx h \times 420$ Hz. After BEC is reached, the sum of the hold time and the ramp time of dipole beam power is 0.8 s. After the 60 Hz line signal decoheres, the feed-forward cancelation does not function, and thus the 60 Hz detuning noise could drive the atoms slightly out of the equilibrium and out of the absolute ground state. Further reduction of bias field noise is needed in order to improve the current measurements.

* Electronic address: linyj@gate.sinica.edu.tw